HHS Public Access

Author manuscript

J Physiol. Author manuscript; available in PMC 2021 February 10.

Published in final edited form as:

J Physiol. 2020 November ; 598(21): 4843–4858. doi:10.1113/JP280232.

Vascular ATP-sensitive K^+ channels support maximal aerobic capacity and critical speed via convective and diffusive O_2 transport

Trenton D. Colburn[1], **Ramona E. Weber**[1], **K. Sue Hageman**[2], **Jacob T. Caldwell**[1], **Kiana M. Schulze**[1], **Carl J. Ade**[1], **Brad J. Behnke**[1], **David C. Poole**[1,2], **Timothy I. Musch**[1,2]

[1]Department of Kinesiology, Kansas State University, Manhattan, KS, 66506, USA

[2]Department of Anatomy and Physiology, Kansas State University, Manhattan, KS, 66506, USA

Abstract

Vascular ATP-sensitive K^+ (K_{ATP}) channels support skeletal muscle blood flow and microvascular oxygen delivery-to-utilization matching during exercise. However, oral sulphonylurea treatment for diabetes inhibits pancreatic K_{ATP} channels to enhance insulin release. Herein we tested the hypotheses that: i) systemic K_{ATP} channel inhibition via glibenclamide (GLI; 10 mg kg^{-1} i.p.) would decrease cardiac output at rest (echocardiography), maximal aerobic capacity ($\dot{V}O_2max$) and the speed–duration relationship (i.e. lower critical speed (CS)) during treadmill running; and ii) local K_{ATP} channel inhibition (5 mg kg^{-1} GLI superfusion) would decrease blood flow (15 μm microspheres), interstitial space oxygen pressures (PO_2is; phosphorescence quenching) and convective and diffusive O_2 transport ($\dot{Q}O_2$ and DO_2, respectively; Fick Principle and Law of Diffusion) in contracting fast-twitch oxidative mixed gastrocnemius muscle (MG: 9% type I+IIa fibres). At rest, GLI slowed left ventricular relaxation (2.11 ± 0.59 *vs.* 1.70 ± 0.23 cm s^{-1}) and decreased heart rate (321 ± 23 *vs.* 304 ± 22 bpm, both $P < 0.05$) while cardiac output remained unaltered (219 ± 64 *vs.* 197 ± 39 ml min^{-1}, $P > 0.05$). During exercise, GLI reduced $\dot{V}O_2max$ (71.5 ± 3.1 *vs.* 67.9 ± 4.8 ml kg^{-1} min^{-1}) and CS (35.9 ± 2.4 *vs.* 31.9 ± 3.1 m min^{-1}, both $P < 0.05$). Local K_{ATP} channel inhibition decreased MG blood flow (52 ± 25 *vs.* 34 ± 13 ml min^{-1} 100 g $tissue^{-1}$) and PO_2is_{nadir} (5.9 ± 0.9 *vs.* 4.7 ± 1.1 mmHg) during twitch contractions. Furthermore, MG $\dot{V}O_2$ was reduced via impaired $\dot{Q}O_2$ and DO_2 ($P < 0.05$ for each). Collectively, these data

Corresponding author T. D. Colburn, MS: Department of Kinesiology, Kansas State University, 920 Denison Avenue, Manhattan, KS 66506. tcolburn@k-state.edu.

Author contributions

TDC, TIM and DCP conceived and designed the study. TDC, REW, KSH, JTC, KMS, CJA, BJB, TIM and DCP acquired, analysed and interpreted the data. TDC prepared the first draft of the manuscript. All authors reviewed and approved the final version of the manuscript and agree to be accountable for all aspects of the work. All individuals listed as authors qualify for authorship, and all individuals who qualify for authorship are listed.

Competing interests

The authors declare that there are no competing interests.

Data availability statement

The data that support the findings of this study are available from the corresponding author upon reasonable request.

Supporting information

Additional supporting information may be found online in the Supporting Information section at the end of the article.

Statistical Summary Document

support that vascular K_{ATP} channels help sustain submaximal exercise tolerance in healthy rats. For patients taking sulfonylureas, K_{ATP} channel inhibition may exacerbate exercise intolerance.

Keywords

exercise tolerance; gastrocnemius; glibenclamide; interstitial space oxygen pressure

Introduction

Sulphonylureas are the most popular second-line anti-diabetic drug prescribed to patients with Type 2 diabetes mellitus (T2DM, Montvida *et al.* 2018), enhancing insulin release from pancreatic beta cells by inhibition of ATP-sensitive potassium (K_{ATP}) channels. This is true irrespective of the increased risk of adverse cardiovascular events (Simpson *et al.* 2006, 2015; Abdelmoneim *et al.* 2016), developing heart failure (HF; McAlister *et al.* 2008; Kristiansen *et al.* 2011) and all-cause mortality (Simpson *et al.* 2015). K_{ATP} channels are metabolic sensors that are also present in neural, vascular (endothelial) and muscle (smooth, cardiac and skeletal) tissue, contributing significantly to the hyperpolarization of membrane potentials via K^+ efflux and subsequent reductions in calcium ion influx. Attention to this category of K^+ channels, and their physiological significance in metabolic control during exercise, has increased with the use of genetic knockout/down models (Flagg *et al.* 2010). However, the use of genetically altered animal models may result in unknown/unrelated systemic modifications and confound the translatability of K_{ATP} channel function to humans (Kane *et al.* 2004).

Current data from animal and human studies modulating K_{ATP} channel function with inhibitors (i.e. glibenclamide (GLI), tolbutamide) and activators (pinacidil) suggest that normal K_{ATP} channel function plays a significant role in limiting myocardial damage following ischaemic events in sedentary and exercise-trained animals (cardiac; Brown *et al.* 2005a,b), enhance reactive and functional hyperaemia to skeletal muscle (vascular; Banitt *et al.* 1996; Bijlstra *et al.* 1996; Saito *et al.* 1996; Hammer *et al.* 2001; Keller *et al.* 2004; Lu *et al.* 2013; Holdsworth *et al.* 2015; but not all, Farouque & Meredith, 2003), and reduce skeletal muscle tension between contractions (myocyte; Gong *et al.* 2000; Matar *et al.* 2000). Whereas systemic administration of GLI has been shown to decrease exercising limb blood flow (Keller *et al.* 2004; Holdsworth *et al.* 2015) and maximal aerobic capacity ($\dot{V}O_2max$; Lu *et al.* 2013), it remains unknown whether these cardiovascular impairments are mediated through reductions in cardiac function, vascular function within skeletal muscle, or both. As adequate energy production via oxidative metabolism dictates contractile function during fatiguing activity and depends on heterogeneous oxygen transport within muscle (Wilson *et al.* 1977; Hogan *et al.* 1992; Richardson *et al.* 1998), maximal oxygen uptake ($\dot{V}O_2max = \dot{Q}max \times$ maximal $a - vO_2$ difference) relies on a prodigious increase in cardiac output ($\dot{Q}$) combined with a highly effective red blood cell distribution and O_2 extraction within active skeletal muscle (arterial–venous O_2 content) (reviewed by Laughlin *et al.* 2012; Poole & Jones, 2012). Notwithstanding the importance of $\dot{V}O_2max$, the ability to sustain high-intensity exercise and daily physical tasks are more appropriately determined via a submaximal threshold (i.e. critical speed (CS) or critical power) where oxidative metabolism

meets metabolic demand below this threshold but, above this threshold, increases infast-twitch fibre recruitment, fatigue-related metabolite production, and O_2 consumption leading to $\dot{V}O_2max$ and task failure (Monod & Scherrer, 1965; Poole *et al.* 1988, 2016; Jones *et al.* 2008; Copp *et al.* 2010). Importantly, it remains unknown how vascular K_{ATP} channels contribute to O_2 transport within highly oxidative fast-twitch muscles and their role in supporting fatiguing exercise, especially as the proportional contribution of these channels to the overall vascular response may increase in disease (Holdsworth *et al.* 2017).

Therefore the current investigation was designed to assess the effect of systemic K_{ATP} channel inhibition via GLI on: i) resting cardiac function; ii) maximal aerobic capacity ($\dot{V}O_2max$); and iii) submaximal exercise tolerance (CS). Local K_{ATP} channel inhibition via GLI superfusion was used to assess: iv) skeletal muscle blood flow ($\dot{Q}m$); and v) interstitial space O_2 pressures (PO_2is; established by O_2 delivery-to-utilization matching immediately proximal to myocytes) within contracting fast-twitch muscle of high oxidative capacity. Incorporating the Fick principle $\left(\dot{V}O_2 = \dot{Q}m \times (CaO_2 - C\upsilon O_2)\right)$ and law of diffusion $\left(\dot{V}O_2 = DO_2 \times \Delta PO_2\right)$ direct measurements were used to estimate convective ($\dot{Q}O_2$) and diffusive (DO_2) O_2 conductances within microvascular and interstitial compartments where the convergence of $\dot{Q}O_2$ and DO_2 establish $\dot{V}O_2$ (Wagner, 1992, 1996). Considering that vascular function and exercise assessments of K_{ATP} channels have been performed in male rats (Lu *et al.* 2013; Holdsworth *et al.* 2015, 2016, 2017) when females may be more adversely affected by sulphonylurea treatment (Brown *et al.* 2005b; Johnson *et al.* 2006), the current investigation sought to bridge the translatability of K_{ATP} channel function to females. It was hypothesized that K_{ATP} channel inhibition would impair resting cardiac output and decrease $\dot{V}O_2max$ and CS. It was further hypothesized that local K_{ATP} channel inhibition would reduce skeletal muscle blood flow and PO_2is during twitch contractions, and slow the recovery of PO_2is following contractions, effectively decreasing $\dot{V}O_2$ by impairing O_2 conductance ($\dot{Q}O_2$ and DO_2). Data in support of these hypotheses would reveal a heretofore under-appreciated peripheral vascular role for K_{ATP} channels in the maintenance of O_2 delivery and contractile function.

Methods

Ethical approval

All protocols and procedures were approved by the Institutional Animal Care and Use Committee of Kansas State University and conducted according to the guidelines and ethical standards put forth by the National Institutes of Health and *Journal of Physiology* (Grundy, 2015). Ten female Sprague–Dawley rats (~8 months old during terminal experiments) were maintained in animal facilities accredited by the Association for the Assessment and Accreditation of Laboratory and Animal Care on a 12:12 h light:dark cycle with food and water provided *ad libitum*. Vaginal lavages were conducted for a minimum of 10 days to monitor menstrual cycles (Marcondes *et al.* 2002; Smith *et al.* 2017) with all testing performed during the pro-oestrus phase. In the initial 14–21 days, while menstrual cycles were monitored, acclimation to running was conducted on a custom-built treadmill for ~5 min day^{-1} at ~25 m min^{-1} up a 5% incline. During the final acclimation days the treadmill

speed was increased progressively in the last 2–3 min up to 50–60 m min^{-1} to familiarize the rats with high-speed running (Copp *et al.* 2010; Craig *et al.* 2019a, Poole *et al.* 2020). Importantly, these brief duration acclimation runs do not elicit training adaptations (Dudley *et al.* 1982; Armstrong & Laughlin, 1984; Musch *et al.* 1992).

Drug dosing

K_{ATP} channel inhibition was administered via the pharmacological sulphonylurea derivative glibenclamide (GLI: 494 g mol^{-1}, 5-chloro-*N*-{4-[*N*-(cyclohexylcarbamoyl)sulfamoyl]phenthyl}−2-methoxybenzamide, Sigma-Aldrich, St. Louis, MO). For acute systemic inhibition via an intraperitoneal injection on experimental days, a 10 ml stock solution was made by GLI dissolved in 9 ml saline (0.9% NaCl), 900 µl NaOH (0.1 m), and 100 µl DMSO and briefly sonicated. The amount of GLI dissolved in solution was determined on experimental days to obtain a final 1 ml dose of 10 mg kg^{-1} (Lu *et al.* 2013). For local inhibition via superfusion, the stock solution utilized distilled water in place of saline and GLI was dissolved to obtain a final 5 mg kg^{-1} dose, with 0.5 ml GLI stock solution diluted in 2.5 ml of warmed Krebs–Hensleit bicarbonate-buffered solution equilibrated with 5% CO_2–95% N_2 (pH 7.4; in mm, 4.7 KCl, 2.0 $CaCl_2$, 2.4 $MgSO_4$, 131 NaCl and 22 $NaHCO_3$).

GLI injections (10 mg kg^{-1}, $_{i.p.}$) occurred ~30–60 min prior to echocardiographic assessment and treadmill exercise testing ($\dot{V}O_2max$ and CS; Lu *et al.* 2013) to align with peak plasma concentration (i.e. ~60–85 min after oral administration of 10 mg kg^{-1} GLI, Li *et al.* 2012). Thus, each rat underwent at least six GLI injections over ~7–8 weeks. During interstitial PO_2 measurements, inhibition was administered locally via GLI superfusion (5 mg kg^{-1} in Krebs–Hensleit solution, Holdsworth *et al.* 2017).

Echocardiography determination of left ventricular function

Transthoracic echocardiography was performed with a commercially available system (Logiq S8; GE Health Care, Milwaukee, WI) using an 18 MHz linear transducer (L8–18i). Rats were anaesthetized initially on a 5% isoflurane–O_2 mixture and then maintained on a 1.5–2% isoflurane–O_2 mixture while positioned supine on a heating pad (42°C) to maintain core temperature. Standard two-dimensional and M-mode images were obtained from the midpapillary level with frame rates >50 frames s^{-1}. Ventricular dimensions were obtained from M-mode measurements over four consecutive cardiac cycles. Left ventricular (LV) internal dimensions were measured at end diastole (LVIDd) and end systole (LVIDs). Fractional shortening (FS) was calculated from LV chamber diameters: FS = [(LVIDd – LVIDs)/LVIDd] × 100. Left end-systolic (LVESV) and end-diastolic (LVEDV) volumes were estimated using the Teichholz formula: LV volume = [7.0/(2.4 + LV dimension)] × LV $dimension^3$. Stroke volume (SV) was calculated as: SV = LVEDV–LVESV. Ejection fraction (EF) was calculated using LV volume measurements: EF = [(LVEDV–LVESV)/LVEDV] × 100. Rates of contraction (+V) and relaxation (−V) of the posterior LV wall were also measured in M-mode by integrating the slope from end-diastolic and end-systolic internal diameter locations used for assessing LVIDd and LVIDs. Heart rate (HR) was estimated using the average contraction and relaxation times across the four cardiac cycles: HR = 60/

(contraction time + relaxation time). Cardiac output (CO) was calculated using HR and SV values: CO = HR × SV.

Determination of maximal oxygen uptake and critical speed

Maximal oxygen uptake ($\dot{V}O_2max$) tests were performed in a plexiglass metabolic chamber placed on the treadmill (Musch *et al.* 1988) and connected to O_2 (model S-3A/I) and CO_2 (model CD-3A; AEI Technologies; Pittsburg, PA) analysers. Gas measurements were performed in real time and recorded in the final 5–10 s of each stage. Treadmill speed was initially set to 25 m min^{-1} for 2 min, increased to 40 m min^{-1} for an additional 2 min, and then increased progressively ~5 m min^{-1} each minute until the rat was unable to maintain pace with the treadmill or no further increases in $\dot{V}O_2$ were recorded despite increases in speed. High reproducibility of $\dot{V}O_2max$ measurements has been established previously in our laboratory (Copp *et al.* 2009).

Following $\dot{V}O_2max$ testing, the speed–duration relationship was determined via the multiple constant-speed method (Copp *et al.* 2010; Craig *et al.* 2019a). Critical speed tests consisted of five runs-to-exhaustion at predetermined speeds estimated to elicit exhaustion between 2 and 20 min. Each test began with a 2 min warm-up at 20 m min^{-1}, followed by 1 min of quiet rest, and then rapid increase in treadmill speed (<10 s) toward the target speed to be maintained for the duration of the test. Timing began when the investigator adjusting treadmill speed verified the attainment of the target speed. When rats drifted toward the back of the running lane a separate investigator provided encouragement via manual bursts of air toward the hindlimbs. Tests were terminated immediately when rats were unable to keep up with the treadmill speed despite apparent exertion and encouragement. The termination of all tests was determined by the same investigators who were blinded to the overall exercise time. Successful runs-to-exhaustion were verified by the absence of a righting reflex (i.e. unwilling/unable to right themselves within 2 s of being placed on their backs). The initial run was set at 60 m min^{-1} and subsequent speeds were selected at ~5 m min^{-1} increments to obtain the appropriate range of run durations (i.e. 2–20 min). When successful constant-speed tests were completed, the speed–duration parameters were determined by: 1) the hyperbolic speed–time model (time = D'/(speed - CS), where the asymptote of this curve is CS and the curvature constant is D'; and 2) the linear 1/time model (speed = D' × 1/time + CS), where speed is plotted as a function of the inverse of time (s) to exhaustion, D' is the slope, and CS is the intercept of the regression line (Copp *et al.* 2010, 2013; Poole *et al.* 2016). To mitigate any potential influence of training (increased CS) or weight gain (decreased CS) on the speed–duration relationship, the slowest of the constant-speed runs were performed early (i.e. run 2–4) under control conditions and the final runs overall consisted of control and GLI runs at the slowest speeds. Preliminary data showed that times-to-exhaustion of the slowest speed under control conditions, and thus CS, were either maintained or decreased compared with the initial slowest run. Therefore the shorter of the two was used to model the speed–duration relationship.

Phosphorescence quenching determination of PO_2*is*

On the final day of experimentation, rats were anaesthetized initially on a 5% isoflurane–O_2 mixture and maintained on 2–2.5% isoflurane–O_2 mixture for the duration of carotid and caudal (tail) artery catheterizations and surgical exposure of hindlimb muscles. Rats were placed on a heating pad to maintain core temperature at ~37–38°C, measured via rectal thermometer. Following a midline incision of the skin covering the neck, the right carotid artery was isolated and cannulated (PE-10 connected to PE-50; Intra-Medic polyethylene tubing; BD, Franklin Lakes, NJ, USA) for continuous measurements of mean arterial pressure (MAP) and HR, and infusion of fluorescent-labelled microspheres for blood flow measurements (see *Fluorescent microsphere assessment of blood flow*). The caudal artery was cannulated for infusion of pentobarbital sodium anaesthesia and blood sampling (i.e. blood gases and blood flow reference sample). Arterial blood samples were collected following the final contraction protocol for determination of O_2 saturation, systemic haematocrit and plasma lactate (Nova Stat Profile M; Nova Biomedical, Waltham, MA, USA).

Following catheterization, an incision was made above the lateral malleolus of the left hindlimb and the overlaying skin and fascia reflected to expose the biceps femoris. Upon tying off the lateral great saphenous artery (6–0 silk suture) the distal portion of the biceps femoris was reflected to expose the mixed gastrocnemius (MG). The MG muscle was selected for its fast-twitch fibre composition (97% type IIA+IID/X+IIB), oxidative capacity (citrate synthase: ~25 μmol min^{-1} g^{-1}; Armstrong & Phelps, 1984; Delp & Duan, 1996), and most importantly its recruitment at and above the fatigue threshold (i.e. CS; Copp *et al.* 2010). The MG was left attached to its anatomical origin and insertion while variations in muscle length were minimized throughout the experimental protocol with knee and ankle joints stabilized ~90° angles. Rats were then progressively transitioned off isoflurane and onto pentobarbital sodium anaesthesia (50 mg ml^{-1}) with the depth of anaesthesia continuously monitored via toe pinch and corneal sensitivity reflexes, and additional anaesthesia provided as necessary (0.03–0.05 ml of 50 mg ml^{-1} diluted to 0.3 ml of heparinized saline). Platinum iridium electrodes were attached (6–0 silk suture) to the proximal (cathode) and distal (anode) regions of the muscles to produce electrically induced muscle contractions. Surrounding exposed tissue was covered with Saran Wrap (Dow Brands, Indianapolis, IN) to reduce tissue dehydration and exposure to superfused solutions. Exposed muscle was superfused regularly with warmed Krebs–Henseleit bicarbonate-buffered solution equilibrated with 5% CO_2–95% N_2.

Experimental protocol.—Two separate contraction bouts were performed on the MG under control (Krebs–Heneseleit) and K_{ATP} channel inhibition (5 mg kg^{-1} GLI in Krebs–Henseleit) superfused conditions. GLI superfusion was performed second, due to the long half-life of GLI, and with >20 min of recovery between contraction bouts to prevent any potential priming effect of repeated contraction bouts on PO_2*is* profiles. Interstitial space PO_2 (PO_2*is*) was measured via phosphorescence quenching at rest and during 180 s twitch contractions (1 Hz, 7 V, 2 ms pulse duration; Grass stimulator model S88, Quincy, MA) and recorded at 2 s intervals (Craig *et al.* 2018, 2019a,b, Hirai *et al.* 2018a). Recovery PO_2*is* was measured for an additional 240 s to ensure that PO_2*is* returned and stabilized at baseline

prior to subsequent GLI superfusion and contractions. With PO_2is measured continuously, GLI was superfused (3 ml total volume) onto the MG for 180 s and allowed an additional 180 s before the same contraction protocol was repeated (i.e. total of >23 min elapsed between contraction bouts).

Measurement of interstitial PO_2.—A frequency domain phosphorometer (PMOD 5000; Oxygen Enterprises, Philadelphia, PA) was used to measure PO_2is as described previously (Craig *et al.* 2018, 2019a,b, Hirai *et al.* 2018a). The Oxyphor G4 (Pd-*meso*-tetra-(3,5-dicarboxyphenyl)-tetrabenzoporphyrin) was injected locally (2–4 10 µl injections at 10 µm concentration) with a 29 gauge needle, with care taken to avoid any visible vasculature. Following injection, the muscle was covered in Saran Wrap and allowed >20 min to allow the G4 to thoroughly diffuse throughout the interstitial space. This oxyphor is well suited for use in biological tissues because it does not cross membranes and is stable across the physiological pH range (Esipova *et al.* 2011). Muscle surface temperature was measured via non-contact infrared thermometer, since this oxyphor is temperature sensitive. The exposed MG temperatures were 31.6 ± 0.2°C. Previous studies have shown that the present twitch contraction protocol does not significantly change muscle temperature (Craig *et al.* 2018, 2019a).

Phosphorescence quenching applies the Stern–Volmer relationship (Rumsey *et al.* 1988; Esipova *et al.* 2011) describing the quantitative O_2 dependence of the phosphorescent probe G4 via the equation $PO_2is=[(\tau_0/\tau)-1]/(k_Q\cdot\tau_0)$, where k_Q is the quenching constant and τ and τ_0 are the phosphorescence lifetimes at the ambient O_2 concentration and in the absence of O_2, respectively. For G4 in tissue at ~32°C, k_Q is ~258 mmHg/s and τ_0 is ~226 µs (Esipova *et al.* 2011). Because muscle temperature does not change appreciably throughout the contraction protocol used herein (Craig *et al.* 2018, 2019a), the phosphorescence lifetime is determined exclusively by the O_2 partial pressure. Following G4 injection, the common end of the bifurcated light guide was positioned 3–4 mm above the exposed muscle surface. All PO_2is measurements were performed in a dark room to minimize extraneous exposure to light.

Analysis of interstitial PO_2 kinetics.—Contracting PO_2is responses were analysed using 30 s of resting data and the 180 s contraction bouts using a monoexponential plus time delay model (one component) or a monoexponential plus time delay with a secondary component (two component) model when necessary,

One component

$$PO_2is_t = PO_2is_{BL} - \Delta_1 PO_2is\left(1 - e^{-(t - TD)/\tau}\right)$$

Two component

$$PO_2is_t = PO_2is_{BL} - \Delta_1 PO_2is\left(1 - e^{-(t - TD)/\tau}\right) + \Delta_2 PO_2is\left(1 - e^{-(t - TD_2)/\tau_2}\right)$$

where PO_2is_t represents the PO_2is at any point in time, PO_2is_{BL} is the baseline before the onset of contractions, Δ_1PO_2is and Δ_2PO_2is are the primary and secondary amplitudes, TD and TD_2 are the time delays before the fall and secondary rise in PO_2is, and τ and τ_2 are the time constants (i.e. the time required to reach 63% of the amplitude) for the primary and secondary amplitudes. The mean response time (MRT) was calculated as the sum of the model-derived TD and τ. When the secondary component model was necessary, the primary amplitude was constrained to the nadir value in order to maximize the accuracy of the primary response kinetics (Craig *et al.* 2018, 2019a,b). The goodness of model fit was determined using the following criteria: 1) coefficient of determination, 2) sum of the squared residuals, and 3) visual inspection and analysis of the model fits to the data and the residuals. Because Δ_2PO_2is (i.e. undershoot of PO_2is; $\Delta_2PO_2is = PO_2is_{end} - PO_2is_{nadir}$) was often non-exponential in nature, Δ_2PO_2is was determined manually by calculating the difference between the PO_2is at the end of contractions (PO_2is_{end}, average of 172–180 s) minus the nadir value of PO_2is during contractions ($PO_2is_{nadir} = PO_2is_{BL} - \Delta_1PO_2is$). Rate of PO_2is recovery was calculated in eight rats as the time taken to reach 63% of the overall response (i.e. T63) between PO_2is_{end} and recovery PO_2is (average of 232–240 s).

Fluorescent microsphere determination of blood flow

The microsphere technique was used to determine MG blood flow as described previously (Musch *et al.* 1986; Van Oosterhout *et al.* 1998; Deveci & Egginton, 1999). Two fluorescent microspheres (blue-green (430/465 nm) and red (580/605 nm), Invitrogen FluoSpheres polystyrene microspheres, ThermoFisher Scientific) were injected in random order at the end of MG and MG GLI contractions. Following 180 s contractions, blood withdrawal from the tail catheter was initiated at 0.25 ml min^{-1} while 0.25–0.30 × 10^6 15.5 μm diameter fluorescent microspheres were injected into the aortic arch via the carotid artery catheter. Muscle contractions and blood withdrawal were terminated 30 s after the microsphere injection. Following the final contraction protocol, rats were killed via pentobarbital sodium overdose (>100 mg kg^{-1} i.a.), proper catheter placement in the aortic arch was confirmed, and tissues (left and right kidneys, left and right mixed gastrocnemei) dissected and stored (−80°C) for later analyses. For the final analyses, kidney and muscle tissues were weighed and placed directly in 15 ml screw cap polypropylene tubes with a conical base. Five ml of 2 M KOH in 99% ethanol with 0.5% Tween-80 were added to the tubes, vortexed, and placed in a dry heating block (60°C) with intermittent vortexing until tissue digestion was complete. Tubes were then centrifuged at 3000 rpm (1500 *g*) for 15 min. Supernatant was carefully aspirated until <500 μl remained to minimize the possibility of accidental microsphere loss. One ml of deionized H_2O was added and tubes quickly vortexed to resuspend the remaining pellet, followed by the addition of 9 ml ethanoic Tween-80, vortexing and another 15 min of centrifuging. Tubes were aspirated as previously described, before 5 ml of 100 mm phosphate buffer (pH 7.0) was added to neutralize the pellet and solution, followed by 4 ml of absolute ethanol. The tubes were further vortexed, centrifuged, and aspirated to <300 μl. To ensure complete resuspension of microspheres, the tubes were vortexed again before being placed in an oven (60°C) to evaporate to 100–150 μl. To improve solvent extraction from the microspheres, which would be less efficient in a dry pellet, the tubes were periodically removed from the oven and vortexed. To dissolve the polystyrene microspheres and release the fluorescent dye, 2 ml of solvent (di(ethylene glycol) ethyl ether acetate, 98%;

Sigma-Aldrich Corporation, St. Louis, MO, USA) was added and vortexed several times over 3–5 min and left for 30 min before being sonicated (5 min) in a water bath to ensure complete dye extraction. Once the solvent was added, all remaining steps were conducted in dim lighting to prevent signal decay prior to fluorescent intensity measurements. After sonication the tubes were centrifuged once more (10 min) before supernatant was pipetted (300 μl) into 96 well plates in quadruplicates for the measurement of fluorescent intensity (SpectraMax i3 Multi-Mode Platform, Molecular Devices, San Jose, CA). Total tissue blood flows were calculated according to the reference sample method (Ishise *et al.* 1980; Musch & Terrell, 1992) and expressed mass specifically in ml min^{-1} 100g $tissue^{-1}$. Adequate mixing of microspheres prior to infusion were determined by <20% difference in left and right kidney and/or muscle blood flows.

Muscle oxygen consumption

The Fick equation was used to calculate microvascular oxygen consumption $(\dot{V}O_2mv)$ with the assumptions that microvascular PO_2 (PO_2mv) can be calculated from interstitial measurements (i.e. $PO_2mv = PO_2is +$ transcapillary PO_2; Colburn *et al.* 2020a) and is an appropriate analogue for venous PO_2 (McDonough *et al.* 2001) and, by extension from the O_2 dissociation curve, venous blood O_2 content (Roca *et al.* 1992). Therefore mixed venous O_2 content (CvO_2) was calculated from PO_2mv using the rat O_2 dissociation curve (constructed using the Hill coefficient (n) of 2.6, the measured [Hb], P_{50} (the PO_2 at which Hb is 50% saturated with O_2) of 38 mmHg, and an O_2-carrying capacity of 1.34 ml O_2 $(gHb)^{-1}$). Arterial O_2 content (CaO_2) was measured directly via arterial blood sample and, when combined with blood flow ($\dot{Q}m$) and CvO_2 values, was used to calculate $\dot{V}O_2mv$ via the principle of mass balance using the Fick Equation (i.e. $\dot{V}O_2mv = \dot{Q}m \times (CaO_2 - CvO_2)$). Microvascular O_2 diffusion conductance (DO_2mv) was defined as $\dot{V}O_2mv/PO_2mv$ which provides an index of diffusive O_2 transport per unit of driving pressure. Interstitial O_2 diffusion conductance $(DO_2is = \dot{V}O_2is/PO_2is)$ was assessed utilizing the present PO_2is and calculated $\dot{V}O_2mv$ (i.e. $\dot{V}O_2is$ was presumed to be equal to $\dot{V}O_2mv$ considering the absence of storage for O_2 in the interstitial fluid and, thus, O_2 leaving the microvascular compartment must equal O_2 leaving the interstitial compartment).

Statistical analyses

The effect of systemic GLI on resting LV function, exercise parameters ($\dot{V}O_2max$, CS and D′), and local GLI superfusion on contracting MG measurements (MAP, HR, PO_2is kinetics parameters, $\dot{Q}m$, microvascular $\dot{Q}O_2$ and $\dot{V}O_2$ and microvascular and interstitial DO_2) were assessed using two-tail paired t tests. PO_2is profiles were assessed via two-way repeated measure ANOVA (Time × Drug) with Tukey's *post hoc* analyses. Data are presented as means ± SD. Significance was accepted at $P < 0.05$.

Results

Two rats were unwilling to complete all runs needed to assess the speed–duration relationship; therefore, comparisons between control and K_{ATP} channel inhibition were conducted on eight rats.

Resting echocardiography

Left ventricular echocardiographic measurements are presented in Table 1. Compared with control, GLI did not alter LVEDV (0.83 ± 0.24 *vs.* 0.83 ± 0.18, $P = 0.976$) nor LVESV (0.15 ± 0.07 *vs.* 0.19 ± 0.09 ml, $P = 0.172$) and thus stroke volume remained unchanged (0.68 ± 0.19 *vs.* 0.65 ± 0.11 ml, $P = 0.354$). LV fractional shortening (47 ± 6 *vs.* 42 ± 5, $P = 0.084$) and EF (83 ± 5 *vs.* 78 ± 6%, $P = 0.088$) were also not significantly altered. However, the rate of LV relaxation (2.11 ± 0.59 *vs.* 1.70 ± 0.23, $P = 0.048$), but not contraction (2.76 ± 0.49 *vs.* 2.44 ± 0.43 cm s^{-1}, $P = 0.079$), was significantly slowed resulting in a decreased HR (321 ± 23 *vs.* 304 ± 22 bpm, $P = 0.043$) during maintained cardiac output (219 ± 64 *vs.* 197 ± 39 ml min^{-1}, $P = 0.105$).

Maximal aerobic capacity and speed–duration relationship

Table 2 and Figs 1 and 2 demonstrate that GLI reduced $\dot{V}O_2max$ (71.5 ± 3.1 *vs.* 67.9 ± 4.8 ml min^{-1} kg^{-1}, $P = 0.034$) and CS (35.9 ± 2.4 *vs.* 31.9 ± 3.1 m min^{-1}, $P = 0.020$) whereas D′ remained unchanged (98 ± 16 *vs.* 91 ± 25 m, $P = 0.532$).

Blood sample analysis and central haemodynamics during phosphorescence quenching

Arterial pH (7.39 ± 0.03), O_2 saturation (90.7 ± 2.6%), haematocrit (34.9 ± 4.2%) and lactate concentration (1.5 ± 0.5 mm) were assessed following the GLI contraction. GLI superfusion did not alter MAP or HR (both $P > 0.346$); therefore, MAP (102 ± 10 and 99 ± 10 mmHg, $P = 0.096$) and HR (361 ± 23 and 364 ± 38 bpm, $P = 0.831$) were not different at the start of the control and GLI contractions, respectively.

MG blood flow and interstitial PO_2

GLI superfusion impaired MG blood flow during contractions (52 ± 25 *vs.* 34 ± 13 ml min^{-1} 100 g^{-1}, $P = 0.015$). The effect of GLI superfusion on PO_2is during the rest–contraction transient is presented in Table 3 and Fig. 3. GLI reduced MG PO_2is_{BL} (−1.1 ± 1.1 mmHg, $P = 0.020$). At the onset of contractions, there was a shortening in TD ($P = 0.005$) with a statistically non-significant change in τ (14.1 ± 2.7 *vs.* 12.2 ± 3.0, $P = 0.053$) yet a faster overall PO_2is fall (MRT: 22.2 ± 4.7 *vs.* 17.3 ± 4.3 s, $P = 0.002$) to a lower PO_2is_{nadir} (5.9 ± 0.9 *vs.* 4.7 ± 1.1, $P = 0.013$) but not a different PO_2is_{end} (7.3 ± 1.5 *vs.* 6.1 ± 1.4 mmHg, $P = 0.073$) compared with control (see Fig. 3; all 2 s measurements, two-way repeated measures ANOVA with Tukey's *post hoc* analyses, $P < 0.062$). Following contractions, GLI PO_2is recovered more slowly (T_{63}: 95 ± 19 *vs.* 118 ± 20 s, $P = 0.047$) but to a similar end recovery PO_2is (14.6 ± 4.0 *vs.* 15.3 ± 6.5 mmHg, $P = 0.556$) during the observed window.

MG muscle oxygen delivery, consumption and diffusive conductance

Compared with control, Fig. 4 illustrates that GLI decreased MG oxygen delivery ($\dot{Q}O_2mv$: 6.4 ± 3.2 *vs.* 4.2 ± 1.7 ml O_2 min^{-1} 100 g^{-1}, $P = 0.015$) and oxygen consumption from the microvascular compartment ($\dot{V}O_2mv$: 5.8 ± 2.9 *vs.* 3.9 ± 1.6 ml O_2 min^{-1} 100 g^{-1}, $P = 0.016$). Consequently, microvascular (DO_2mv: 0.40 ± 0.20 *vs.* 0.30 ± 0.11, $P = 0.023$) and interstitial diffusive conductances (DO_2is: 0.80 ± 0.38 *vs.* 0.66 ± 0.25 ml O_2 min^{-1} $mmHg^{-1}$ 100 g^{-1}, $P = 0.040$) were significantly reduced. Furthermore, DO_2is was significantly greater than DO_2mv ($P = 0.0002$ and 0.0001, control and GLI, respectively), with the

reduction in DO_2mv following GLI (−22 ± 20%) trending towards being proportionally greater than the reduction in DO_2is (−15 ± 17%; $P = 0.070$).

Discussion

The main original finding of this investigation is that, in female rats, GLI-induced impairment of maximal (i.e. $\dot{V}O_2max$) and submaximal (i.e. CS) exercise can be attributed, in part, to reductions in peripheral vascular K_{ATP} channel function. Systemic GLI administration did not change cardiac output at rest, assessed via Doppler echocardiography. However, the slowed LV relaxation and reduced HR at rest following GLI highlights a peripheral insult to K_{ATP} channels that is likely compensated, in part, by baroreflex-mediated changes in left ventricular function. Accordingly, local inhibition of vascular K_{ATP} channels during contractions resulted in decreased blood flow and interstitial space O_2 delivery-to-utilization matching (i.e. PO_2is) of fast-twitch oxidative skeletal muscle and slowed the recovery of PO_2is following cessation of contractions. Using the Fick principle and law of diffusion, estimations of MG convective and diffusive conductances ($\dot{Q}O_2$ and DO_2, respectively), and thus $\dot{V}O_2$, were impaired following GLI. Therefore, the exercise intolerance that is symptomatic of patient populations (i.e. diabetes, HF), which have a greater proportion of, and blood flow to, fast-twitch fibres, may be exacerbated by oral sulphonylurea medications impairing vascular K_{ATP} channel-mediated vasodilation.

K_{ATP} channel function on maximal aerobic capacity and speed–duration relationship

Consistent with our hypothesis, systemic K_{ATP} channel inhibition impaired maximal aerobic capacity ($\dot{V}O_2max$) and submaximal exercise tolerance (CS). Lu and colleagues (2013) previously demonstrated impaired $\dot{V}O_2max$ (~54 to 36 ml O_2 min^{-1} kg^{-1}, ~33%) in rats following GLI injections; however, utilizing a comparatively steeper ramp protocol, the current data exhibited higher baseline $\dot{V}O_2max$ and a far smaller effect of GLI (~5%, Table 2). This discrepancy likely stems directly from the slower ramp protocol wherein longer durations at submaximal speeds would be expected to enhance glycogen depletion in skeletal muscle leading to exhaustion at lower $\dot{V}O_2$ levels. Supporting the need for steeper ramp protocols, Richardson *et al.* (1993) demonstrated greater $\dot{V}O_2max$ and maximum work rate within 13–15 min of knee extension exercise compared with those previously measured using a slower, longer ramp protocol (~40–60 min; Andersen & Saltin, 1985). Accordingly, GLI-induced reductions in HR in the face of elevated MAP occurred at slower speeds, but not at 60 m min^{-1} (Holdsworth *et al.* 2015). Coupled with decreased hindlimb muscle blood flows throughout all speeds, this suggests that vascular control of O_2 delivery is impaired especially at submaximal speeds while metabolite build-up at supra-CS speeds may activate group III/IV afferents to increase HR at near-maximal speed/intensity (Holdsworth *et al.* 2015). This notion is highlighted in the current investigation (Fig. 1) where GLI-induced reductions in CS were greater than those seen in $\dot{V}O_2max$ (~12 *vs.* ~5%, respectively).

K_{ATP} channel function on cardiac function

Assessed via Doppler ultrasound under anaesthesia, GLI significantly reduced the rates of LV relaxation and HR (Table 1) but not cardiac output. Decreased HR has been

demonstrated in GLI-treated rats during conscious rest which occurred simultaneously with increased MAP and decreased sympathetic activity to hindlimb muscles (Colburn *et al.* 2020b). Although resting cardiac function is not expected to relate directly to cardiac function during high-intensity exercise (Fig. 1), we believe that the present changes in LV relaxation and HR at rest help to emphasize a peripheral insult following systemic K_{ATP} channel inhibition (Holdsworth *et al.* 2015, 2016; Colburn *et al.* 2020b) that manifests changes in cardiac function likely to minimize MAP increases (Colburn *et al.* 2020b) and/or decrease the work of the heart during elevated MAP. Additionally, as direct K_{ATP} channel inhibition of cardiomyocytes would enhance contractility and hinder relaxation (Flagg *et al.* 2010; Kane *et al.* 2005; Zingman *et al.* 2007), it is most likely that the primary effect of systemic GLI administration herein results from a peripheral, and not cardiomyocyte-mediated, alteration in K_{ATP} channel function (i.e. vascular K_{ATP} channel inhibition leading to vasoconstriction and increased MAP with a baroreceptor-mediated secondary reduction in sympathetic activity to decrease cardiac output, Colburn *et al.* 2020b). These adjustments in cardiac function are likely removed at near-maximal exercise intensities when sympathetic activity is enhanced and HR is not different between control and GLI conditions (Holdsworth *et al.* 2015). However, future experimental designs where possible should measure SV and cardiac output during high-intensity exercise to assess the primary, or secondary, effect of K_{ATP} channel inhibition on cardiac function. Nevertheless, reductions in $\dot{V}O_2max$ herein are considered to result, in part, from $\dot{Q}O_2$:$\dot{V}O_2$ mismatch at the level of skeletal muscle and impaired systemic arterial–venous O_2 difference (i.e. $\dot{V}O_2max = \dot{Q}O_2max \times$ maximal $a - vO_2$ difference).

K_{ATP} channel function on skeletal muscle blood flow and PO_2is

To assess the contribution of vascular K_{ATP} channels supporting skeletal muscle O_2 transport, and thus oxidative phosphorylation, the current investigation measured the interstitial space driving pressure of O_2 (PO_2is) during the rest–contractions transient during submaximal contractions, muscle blood flow ($\dot{Q}m$) at the end of contractions, and PO_2is during recovery. Following local GLI administration, PO_2is in the MG fast-twitch oxidative muscle fell faster (i.e. MRT) and to a lower PO_2is (PO_2is_{nadir}; Table 3, Fig. 3) when $\dot{Q}m$ was reduced. Interestingly, because PO_2is_{BL} was also reduced following GLI, the magnitude of PO_2is fall (i.e. Δ_1PO_2is) was unaltered, possibly due to a lowering of intracellular $\dot{V}O_2$ to preserve interstitial-myocyte PO_2 and prevent muscle damage, as proposed by Richmond *et al.* (1999). Therein the 'critical PO_2', the point at which PO_2is ceased to continue falling and the NADH fluorescence signal increased, was ~2.4–2.9 mmHg for mixed-fibre spinotrapezius muscle and may be greater in the more oxidative MG (citrate synthase activity: ~26 *vs.* ~14 μmol min^{-1} g^{-1}; Delp & Duan, 1996). While the exact contribution of lowered $\dot{V}O_2$ (Fig. 4) is unable to be separated completely between low $\dot{Q}O_2$- (via decreased $\dot{Q}m$ which lowered PO_2is and sped the fall in PO_2is) and/or myocyte-mediated $\dot{V}O_2$ lowering, the end result is indeed lower $\dot{V}O_2$ which would increase the reliance on glycolytic energy sources for contractions and production of fatigue-related metabolites (Wilson *et al.* 1977; Hogan *et al.* 1992; Richardson *et al.* 1998).

In addition, despite recovering to a similar PO_2is, GLI significantly slowed the recovery compared with control. All of these findings during local K_{ATP} channel inhibition provide evidence supporting the hypothesis that the reductions in exercise tolerance resulting from systemic GLI administration were due, in part, to impaired O_2 transport at the microvascular level hindering aerobic metabolism within the contracting myocyte (see Convective and diffusive determinants of O_2 transport below) and, especially for repeated bouts of physical activity, increasing the amount of time needed to re-establish muscle PO_2 and replenish muscle energy stores (Haseler *et al.* 1999; Kindig *et al.* 2005).

Convective and diffusive determinants of O_2 transport

Utilizing direct measurements of $\dot{Q}m$, arterial O_2 content (CaO_2), and the O_2 pressures nearest the contracting myocytes (PO_2is) to calculate PO_2mv ($PO_2mv = PO_2is +$ transcapillary PO_2; Colburn *et al.* 2020a), the authors conflated the Fick principle ($\dot{V}O_2mv = \dot{Q}m \times (CaO_2 - CvO_2)$; i.e. convective O_2 transport) and Fick's law of diffusion ($\dot{V}O_2\,mv = DO_2\,mv \times PO_2\,mv$; i.e. diffusive O_2 transport) to estimate muscle convective O_2 delivery ($\dot{Q}O_2mv$), diffusive conductance for O_2 (DO_2mv), and the resulting $\dot{V}O_2$ from the microvascular compartment. Importantly, the convergence of the convective and diffusive determinants to O_2 transport describes the rate of O_2 consumption by skeletal muscle (Wagner, 1992, 1996).

In the current investigation, impaired PO_2is was due, in part, to reductions in $\dot{Q}m$. As a result, the rate of O_2 able to be consumed from the microvascular compartment was significantly reduced $\dot{V}O_2mv$. As demonstrated in Fig. 4, this change in $\dot{V}O_2mv$ was not only a consequence of impaired $\dot{Q}O_2mv$ ($\downarrow$ 34%) but also lowered microvascular-myocyte diffusing conductance (DO_2mv ↓25%). Traditionally interpreted in the context of microvascular-myocyte O_2 transport, DO_2mv is altered via changes in capillary haematocrit, red blood cell (RBC) flux and RBC velocity (reviewed by Poole *et al.* 2013; Poole, 2019). More recently, with the advent of PO_2is measurements during contractions (Hirai *et al.* 2018a; Colburn *et al.* 2020a), interstitial DO_2 (DO_2is, interstitial-myocyte) can be estimated presuming that O_2 leaving the microvascular compartment ($\dot{V}O_2mv$) equals O_2 leaving the interstitial compartment ($\dot{V}O_2is$; i.e. negligible change in storage of O_2 in interstitial fluid) during steady-state contractions and can be calculated from $\dot{V}O_2mv$ and the present PO_2is (i.e. $DO_2is = \dot{V}O_2mv/PO_2is$ when $\dot{V}O_2mv = \dot{V}O_2is$). Interestingly, since $\dot{V}O_2$ must be equivalent in both compartments, DO_2 was greater in the interstitial compartment compared with microvascular compartment and both decreased with GLI. However, with GLI, DO_2 was almost reduced to a significantly greater extent when O_2 diffused out of the microvascular compartment compared with the subsequent O_2 diffusion out of the interstitium (↓25% and 19%, DO_2mv *vs.* DO_2is, respectively). These disparate magnitudes of, and potential reductions in, DO_2 between compartments are likely to result from: i) divergent surface areas for O_2 flux (i.e. across capillary wall < into myocyte); and ii) fluid dynamics wherein impaired buffering of RBCs following GLI (i.e. ↓ percent capillaries flowing, RBC flux and RBC velocity, Hirai *et al.* 2018b) would yield greater decrements in DO_2mv than DO_2is considering interstitial fluid volume is expected to remain relatively

constant during contractions and unaffected by GLI. Furthermore, since PO_2mv for control and GLI conditions were calculated using the same transcapillary PO_2 ($PO_2mv = PO_2is +$ transcapillary PO_2), the reduction in DO_2mv following GLI is potentially underestimated as a result of increased transcapillary PO_2. Crucially, increased $\dot{Q}m$ and RBC dynamics increase DO_2mv and reduce transcapillary PO_2 (PO_2mv-PO_2is) in the contracting fast-twitch oxidative MG (MG Control: $\uparrow \dot{V}O_2 = \uparrow \uparrow DO_2 \times \downarrow [PO_2mv - PO_2is]$; Colburn *et al.* 2020a) whereas the GLI-induced reduction in $\dot{Q}m$ herein and impaired RBC dynamics (Hirai *et al.* 2018b) would serve to reduce DO_2mv compared with control and therefore increasing the actual PO_2mv following GLI (MG+GLI compared with MG Control: $\downarrow \dot{V}O_2 = \downarrow \downarrow DO_2 \times \uparrow [PO_2mv - PO_2is]$).

The interplay between convective and diffusive O_2 delivery on muscle $\dot{V}O_2$ has been assessed directly in healthy skeletal muscle across fibre types (Behnke *et al.* 2003; McDonough *et al.* 2005), during handgrip exercise (Rosenberry *et al.* 2019) and in disease populations during isolated knee extensor and cycling exercise (chronic obstructive pulmonary disease: Broxterman *et al.* 2020; HFrEF: Esposito *et al.* 2010, 2011 (exercise trained)). To our knowledge, the current investigation is the first to assess changes in convective and diffusive O_2 conductance following specific channel/enzyme inhibition and provides evidence that this approach can be utilized in future studies examining O_2 transport in health, dysfunction related to a range of cardiovascular diseases (i.e. diabetes, sickle cell anaemia, pulmonary hypertension, HF; Padilla *et al.* 2006, 2007; Hirai *et al.* 2015; Ferguson *et al.* 2018), and potential therapeutic interventions aimed at increasing O_2 delivery (i.e. nitrate and nitrite supplementation; Ferguson *et al.* 2013a,b, 2015, 2016a,b; Glean *et al.* 2015; Colburn *et al.* 2017; Craig *et al.* 2019b).

Experimental considerations

Glycolytic muscle fibres experience the greatest metabolic perturbations during exercise and accordingly contain a greater content of pore-forming K_{ATP} channel subunit Kir6.2 (type IIB > IIX > IIA > I; Banas *et al.* 2011) which depresses force production and resting tension and limits intracellular calcium-mediated fibre damage (Gong *et al.* 2003; Thabet *et al.* 2005; Cifelli *et al.* 2008). When skeletal muscle K_{ATP} channels are inhibited via GLI, this could potentially lead to greater myocyte contraction and $\dot{V}O_2$. Although augmenting K_{ATP} channels via pinacidil impairs force production and increases the rate of skeletal muscle fatigue *ex vivo*, K_{ATP} channel inhibition via GLI does not decrease skeletal muscle fatigue or alter force production during tetanic contractions yet appears to increase resting muscle tension between contractions and could, therefore, increase $\dot{V}O_2$ accordingly (Gong *et al.* 2000; Matar *et al.* 2000). Nonetheless, the topical application of GLI and related disturbance of $\dot{Q}O_2$:$\dot{V}O_2$ matching (i.e. PO_2is) of the fast-twitch oxidative glycolytic MG are, principally, consequent to impaired blood flow (decreased herein, and also in Holdsworth *et al.* 2015) rather than increased metabolic demand ($\dot{V}O_2$; see Fig. 4).

Whereas the present experimental design precluded the assessment of blood flow at rest and during treadmill running (i.e. utilizing fluorescent microspheres to assess resting/running blood flow would prevent blood flow assessment during PO_2is in the same rat), prior

investigations from our laboratory have demonstrated reduced muscle blood flow following GLI at rest and a wide range of speeds (20, 40 and 60 m min^{-1}, the latter of which yields $\dot{V}O_2max$ on the inclined treadmill in rats, Colburn *et al.* 2020b and Holdsworth *et al.* 2015). Therefore, the authors are assured that skeletal muscle blood flow is reduced following systemic GLI administration herein and during the cardiac assessment via Doppler ultrasound.

Clinically, a primary concern of sulphonylurea use in patient populations is the potential for hypoglycaemia. Prior to exercise, hypoglycaemia following GLI-mediated insulin release and systemic glucose uptake would inherently limit exercise duration by restricting blood glucose stores available for energy production. To minimize this concern, the authors performed all exercise testing within 30–90 min of systemic GLI administration to target K_{ATP} channel inhibition and not incur the confounding effects on glucose availability that would result from a longer duration GLI-mediated insulin release (Li *et al.* 2012). Importantly, while assessing the speed–duration relationship (Table 2 and Fig. 2), the curvature constant (D') remained unchanged following K_{ATP} channel inhibition. While CS is better understood and reflects the upper threshold of oxidative phosphorylation to support metabolic demand, D' is considered to reflect principally the contributions of finite non-aerobic energy stores and fatigue-resistant muscular properties supporting exercise above CS (reviewed by Poole *et al.* 2016). Additionally, exercise measurements were performed every 4 days to target the pro-oestrus phase. Repeated acute doses of GLI, which has a half-life of up to 10 h, is not anticipated to have a cumulative effect across testing days. Nevertheless, if a chronic K_{ATP} channel inhibition effect was captured, it would mirror more directly the use of oral sulphonylureas in T2DM patients and the present investigation may actually underestimate the long-term effects of K_{ATP} channel inhibition that is associated with elevated risk for adverse cardiovascular events, developing HF, and all-cause mortality (Simpson *et al.* 2006, 2015; McAlister *et al.* 2008; Kristiansen *et al.* 2011; Abdelmoneim *et al.* 2016).

Conclusions

These data emphasize the important role that vascular ATP-sensitive K^+ (K_{ATP}) channels have in supporting exercise tolerance. Crucially, systemic inhibition of K_{ATP} channels via GLI reduces $\dot{V}O_2max$ and submaximal exercise tolerance (CS). These impairments during treadmill running are reflected in fast-twitch oxidative glycolytic MG muscle where local inhibition of vascular K_{ATP} channels reduces skeletal muscle blood flow $\dot{Q}m$ and O_2 delivery during twitch contractions (i.e. PO_2is). As a result, by reducing convective O_2 $\left(\dot{V}O_2 = \dot{Q}m \times \text{ arterial–venous } O_2 \text{ content}\right)$ and diffusive O_2 conductances $\left(\dot{V}O_2 = DO_2 \times \Delta PO_2\right)$, K_{ATP} channel inhibition lowered muscle $\dot{V}O_2$. Therefore, the exercise (in)tolerance of disease patients taking oral sulphonylurea medication may be, in part, due to pharmacologically mediated impairments in vascular O_2 transport and muscle O_2 utilization.

Supplementary Material

Refer to Web version on PubMed Central for supplementary material.

Acknowledgements

We thank Dr Mark Weiss for technical instruction and assistance with vaginal lavage imaging.

Funding

This work was supported by National Institutes of Health (NIH) grants HL-137156-01 (BJB and DCP) and HL-2-108328 (DCP) and Ruth L. Kirschstein National Research Service Award F31HL145981 (TDC).

Biography

Trenton D. Colburn is a Predoctoral Fellow in the Cardiorespiratory Physiology Laboratory at Kansas State University, mentored by Drs Timothy I. Musch and David C. Poole. His research focuses on the regulation of oxygen delivery and utilization within the microvascular and interstitial compartments of skeletal muscle in health and disease, with particular interest in nitric oxide bioavailability and ATP-sensitive potassium channel function during exercise.

References

Abdelmoneim AS, Eurich DT, Senthilselvan A, Qiu W & Simpson SH (2016). Dose-response relationship between sulphonylureas and major adverse cardiovascular events in elderly patients with type 2 diabetes. Pharmacoepidemiol Drug Saf 25, 1186–1195. [PubMed: 27102581]

Andersen P & Saltin B (1985). Maximal perfusion of skeletal muscle in man. J Physiol 366, 233–249. [PubMed: 4057091]

Armstrong RB & Laughlin MH (1984). Exercise blood flow patterns within and among rat muscles after training. Am J Physiol 246, H59–H68. [PubMed: 6696089]

Banas K, Clow C, Jasmin BJ & Renaud JM (2011). The K_{ATP} channel Kir6.2 subunit content is higher in glycolytic than oxidative skeletal muscle fibers. Am J Physiol Regul Integr Comp Physiol 301, R916–R925. [PubMed: 21715697]

Banitt PF, Smits P, Williams SB, Ganz P & Creager MA (1996). Activation of ATP-sensitive potassium channels contributes to reactive hyperemia in humans. Am J Physiol 271, H1594–1598. [PubMed: 8897956]

Behnke BJ, McDonough P, Padilla DJ, Musch TI & Poole DC (2003). Oxygen exchange profile in rat muscles of contrasting fibre types. J Physiol 549, 597–605. [PubMed: 12692174]

Bijlstra PJ, den Arend JACJ, Lutterman JA, Russel FGM, Thien T & Smits P (1996). Blockade of vascular ATP-sensitive potassium channels reduces the vasodilator response to ischaemia in humans. Diabetologia 39, 1562–1568. [PubMed: 8960843]

Brown DA, Chicco AJ, Jew KN, Johnson MS, Lynch JM, Watson PA & Moore RL (2005a). Cardioprotection afforded by chronic exercise is mediated by the sarcolemmal, and not mitochondrial, isoform of the K_{ATP} channel in the rat. J Physiol 569, 913–924. [PubMed: 16223762]

Brown DA, Lynch JM, Armstrong CJ, Caruso NM, Ehlers LB, Johnson MS & Moore RL (2005b). Susceptibility of the heart to ischaemia-reperfusion injury and exercise-induced cardioprotection are sex-dependent in the rat. J Physiol 564, 619–630. [PubMed: 15718263]

Broxterman RM, Hoff J, Wagner PD & Richardson RS (2020). Determinants of the diminished exercise capacity in patients with chronic obstructive pulmonary disease: looking beyond the lungs. J Physiol 598, 599–610. [PubMed: 31856306]

Cifelli C, Boudreault L, Gong B, Bercier JP & Renaud JM (2008). Contractile dysfunctions in ATP-dependent K^+ channel-deficient mouse muscle during fatigue involve excessive depolarization and Ca^{2+} influx through L-type Ca^{2+} channels. Exp Physiol 93, 1126–1138. [PubMed: 18586858]

Colburn TD, Ferguson SK, Holdsworth CT, Craig JC, Musch TI & Poole DC (2017). Effect of sodium nitrite on local control of contracting skeletal muscle microvascular oxygen pressure in healthy rats. J Appl Physiol 122, 153–160. [PubMed: 27789769]

Colburn TD, Hirai DM, Craig JC, Ferguson SK, Weber RE, Schulze KM, Behnke BJ, Musch TI & Poole DC (2020a). Transcapillary PO_2 gradients in contracting muscles across the fibre type and oxidative continuum. J Physiol 598, 3187–3202. [PubMed: 32445225]

Colburn TD, Holdsworth CT, Craig JC, Hirai DM, Montgomery S, Poole DC, Musch TI & Kenney MJ (2020b). ATP-sensitive K^+ channel inhibition in rats decreases kidney and skeletal muscle blood flow without increasing sympathetic nerve discharge. Respir Physiol Neurobiol 278, 103444. [PubMed: 32330600]

Copp SW, Davis RT, Poole DC & Musch TI (2009). Reproducibility of endurance capacity and $\dot{V}o_2$ peak in male Sprague-Dawley rats. J Appl Physiol 106, 1072–1078. [PubMed: 19213934]

Copp SW, Hirai DM, Musch TI & Poole DC (2010). Critical speed in the rat: implications for hindlimb muscle blood flow distribution and fibre recruitment. J Physiol 588, 5077–5087. [PubMed: 20962004]

Copp SW, Holdsworth CT, Ferguson SK, Hirai DM, Poole DC & Musch TI (2013). Muscle fibre-type dependence of neuronal nitric oxide synthase-mediated vascular control in the rat during high speed treadmill running. J Physiol 591, 2885–2896. [PubMed: 23507879]

Craig JC, Colburn TD, Caldwell JT, Hirai DM, Tabuchi A, Baumfalk DR, Behnke BJ, Ade CJ, Musch TI & Poole DC (2019a). Central and peripheral factors mechanistically linked to exercise intolerance in heart failure with reduced ejection fraction. Am J Physiol Heart Circ Physiol 317, H434–H444. [PubMed: 31225988]

Craig JC, Colburn TD, Hirai DM, Musch TI & Poole DC (2019b). Sexual dimorphism in the control of skeletal muscle interstitial PO_2 of heart failure rats: effects of dietary nitrate supplementation. J Appl Physiol 126, 1184–1192. [PubMed: 30844332]

Craig JC, Colburn TD, Hirai DM, Schettler MG, Musch TI & Poole DC (2018). Sex and nitric oxide bioavailability interact to modulate interstitial PO_2 in healthy rat skeletal muscle. J Appl Physiol 124, 1558–1566. [PubMed: 29369738]

Delp MD & Duan C (1996). Composition and size of type I, IIA, IID/X, and IIB fibers and citrate synthase activity of rat muscle. J Appl Physiol, 80, 261–270. [PubMed: 8847313]

Deveci D & Egginton S (1999). Development of the fluorescent microsphere technique for quantifying regional blood flow in small mammals. Exp Physiol 84, 615–630. [PubMed: 10481220]

Dudley GA, Abraham WM & Terjung RL (1982). Influence of exercise intensity and duration on biochemical adaptations in skeletal muscle. J Appl Physiol Respirat Environ Exercise Physiol 53, 844–850.

Esipova TV, Karagodov A, Miller J, Wilson DF, Busch TM & Vinogradov SA (2011). Two new “protected” oxyphors for biological oximetry: properties and application in tumor imaging. Anal Chem 83, 8756–8765. [PubMed: 21961699]

Esposito F, Mathieu-Costello O, Shabetai R, Wagner PD & Richardson RS (2010). Limited maximal exercise capacity in patients with chronic heart failure: partitioning the contributors. J Am Coll Cardiol 55, 1945–1954. [PubMed: 20430267]

Esposito F, Reese V, Shabetai R, Wagner PD & Richardson RS (2011). Isolated quadriceps training increases maximal exercise capacity in chronic heart failure: the role of skeletal muscle convective and diffusive oxygen transport. J Am Coll Cardiol 58, 1353–1362. [PubMed: 21920265]

Farouque HMO & Meredith IT (2003). Effects of inhibition of ATP-sensitive potassium channels on metabolic vasodilation in the human forearm. Clin Sci 104, 39–46.

Ferguson SK, Glean AA, Holdsworth CT, Wright JL, Fees AJ, Colburn TD, Stabler T, Allen JD, Jones AM, Musch TI & Poole DC (2016a). Skeletal muscle vascular control during exercise: impact of

nitrite infusion during nitric oxide synthase inhibition in healthy rats. J Cardiovasc Pharmacol Ther 21, 201–208. [PubMed: 26272082]

Ferguson SK, Hirai DM, Copp SW, Holdsworth CT, Allen JD, Jones AM, Musch TI & Poole DC (2013a). Effects of nitrate supplementation via beetroot juice on contracting rat skeletal muscle microvascular oxygen pressure dynamics. Respir Physiol Neurobiol 187, 250–255. [PubMed: 23584049]

Ferguson SK, Hirai DM, Copp SW, Holdsworth CT, Allen JD, Jones AM, Musch TI & Poole DC (2013b). Impact of dietary nitrate supplemtation via beetroot juice on exercising muscle vascular control in rats. J Physiol 591, 547–557. [PubMed: 23070702]

Ferguson SK, Harral JW, Pak DI, Redinius KM, Stenmark KR, Schaer DJ, Buehler PW & Irwin DC (2018). Impact of cell-free hemoglobin on contracting skeletal muscle microvascular oxygen pressure dynamics. Nitric Oxide 76, 29–36. [PubMed: 29526566]

Ferguson SK, Holdsworth CT, Colburn TD, Wright JL, Craig JC, Fees A, Jones AM, Allen JD, Musch TI & Poole DC (2016b). Dietary nitrate supplementation: impact on skeletal muscle vascular control in exercising rats with chronic heart failure. J Appl Physiol 121, 661–669. [PubMed: 27445296]

Ferguson SK, Holdsworth CT, Wright JL, Fees AJ, Allen JD, Jones AM, Musch TI & Poole DC (2015). Microvascular oxygen pressures in muscles comprised of different fiber types: impact of dietary nitrate supplementation. Nitric Oxide 48, 38–43. [PubMed: 25280991]

Flagg TP, Enkvetchakul D, Koster JC & Nichols CG (2010). Muscle K_{ATP} channels: recent insights to energy sensing and myoprotection. Physiol Rev, 90, 799–829. [PubMed: 20664073]

Glean AA, Ferguson SK, Holdsworth CT, Colburn TD, Wright JL, Fees AJ, Hageman KS, Poole DC & Musch TI (2015). Effects of nitrite infusion on skeletal muscle vascular control during exercise in rats with chronic heart failure. Am J Physiol-Heart C 309, H1354–H1360.

Gong B, Miki T, Seino S & Renaud JM (2000). A K_{ATP} channel deficiency affects resting tension, not contractile force, during fatigue in skeletal muscle. Am J Physiol Cell Physiol 279, C1351–C1358. [PubMed: 11029282]

Gong B, Legault D, Miki T, Seino S & Renaud JM (2003). K_{ATP} channels depress force production by reducing action potential amplitude in mouse EDL and soleus muscle. Am J Physiol Cell Physiol 285, C1464–C1474. [PubMed: 12917105]

Grundy D (2015). Principles and standards for reporting animal experiments in The Journal of Physiology and Experimental Physiology. J Physiol 593, 2547–2549. [PubMed: 26095019]

Hammer LW, Ligon AL & Hester RL (2001). Differential inhibition of functional dilation of small arterioles by indomethacin and glibenclamide. Hypertension 37, 599–603. [PubMed: 11230341]

Haseler LJ, Hogan MC & Richardson RS (1999). Skeletal muscle phosphocreatine recovery in exercise-trained humans is dependent on O_2 availability. J Appl Physiol 86, 2013–2018. [PubMed: 10368368]

Hirai DM, Craig JC, Colburn TD, Eshima H, Kano Y, Sexton WL, Musch TI & Poole DC (2018a). Skeletal muscle microvascular and interstitial PO_2 from rest to contractions. J Physiol 596, 869–883. [PubMed: 29288568]

Hirai DM, Craig JC, Colburn TD, Tabuchi A, Hageman KS, Musch TI & Poole DC (2018b). Regulation of capillary hemodynamics by K_{ATP} channels in resting skeletal muscle. FASEB J 32, 581.8.

Hirai DM, Musch TI & Poole DC (2015). Exercise training in chronic heart failure: improving skeletal muscle O_2 transport and utilization. Am J Physiol Heart Circ Physiol 309, H1419–H1439. [PubMed: 26320036]

Hogan MC, Arthur PG, Bebout DE, Hochachka PW & Wagner PD (1992). Role of O_2 in regulating tissue respiration in dog muscle working in situ. J Appl Physiol 73, 728–736. [PubMed: 1400003]

Holdsworth CT, Copp SW, Ferguson SK, Sims GE, Poole DC & Musch TI (2015). Acute inhibition of ATP-sensitive K^+ channels impairs skeletal muscle vascular control in rats during treadmill exercise. Am J Physiol Heart Circ Physiol 308, H1434–H1442. [PubMed: 25820394]

Holdsworth CT, Ferguson SK, Colburn TD, Fees AJ, Craig JC, Hirai DM, Poole DC & Musch TI (2017). Vascular K_{ATP} channels mitigate severe muscle O_2 delivery-utilization mismatch during

contractions in chronic heart failure rats. Respir Physiol Neurobiol 238, 33–40. [PubMed: 28119150]

Holdsworth CT, Ferguson SK, Poole DC & Musch TI (2016). Modulation of rat skeletal muscle microvascular O_2 pressure via K_{ATP} channel inhibition following the onset of contractions. Respir Physiol Neurobiol 222, 48–54. [PubMed: 26592147]

Ishise S, Pegram BL, Yamamoto J, Kitamura Y & Frohlich ED (1980). Reference sample microsphere method: cardiac output and blood flows in conscious rat. Am J Physiol Heart Circ Physiol 239, H443–H449.

Johnson MS, Moore RL & Brown DA (2006). Sex differences in myocardial infarct size are abolished by sarcolemmal K_{ATP} channel blockade in rat. Am J Physiol-Heart C 290, H2644–H2647.

Jones AM, Wilkerson DP, DiMenna F, Fulford J & Poole DC (2008). Muscle metabolic responses to exercise above and below the “critical power” assessed using 31P-MRS. Am J Physiol Regul Integr Comp Physiol 294, R585–R593. [PubMed: 18056980]

Kane GC, Behfar A, Yamada S, Perez-Terzic C, O’Cochlain F, Reyes S, Dzeja PP, Miki T, Seino S & Terzic A (2004). ATP-sensitive K^+ channel knockout compromises the metabolic benefit of exercise training, resulting in cardiac deficits. Diabetes 53, S169–S175. [PubMed: 15561907]

Kane GC, Liu XK, Yamada S, Olson TM & Terzic A (2005). Cardiac K_{ATP} channels in health and disease. J Mol Cell Cardiol 38, 937–943. [PubMed: 15910878]

Keller DM, Ogoh S, Greene S & Raven PB (2004). Inhibition of K_{ATP} channel activity augments baroreflex-mediated vasoconstriction in exercising human skeletal muscle. J Physiol 561, 273–282. [PubMed: 15345750]

Kindig CA, Walsh B, Howlett RA, Stary CM & Hogan MC (2005). Relationship between intracellular PO_2 recovery kinetics and fatigability in isolated single frog myocytes. J Appl Physiol 98, 2316–2319. [PubMed: 15691906]

Kristiansen SB, Løfgren B, Nielsen JM, Støttrup NM, Buhl ES, Nielsen-Kudsk JE, Nielsen TT, Rungby J, Flyvbjerg A & Bøtker HE (2011). Comparison of two sulfonylureas with high and low myocardial K_{ATP} channel affinity on myocardial infarct size and metabolism in a rat model of type 2 diabetes. Diabetologia 54, 451–458. [PubMed: 21104069]

Laughlin MH, Davis MJ, Secher NH, van Lieshout JJ, Arce-Esquivel AA, Simmons GH, Bender SB, Padilla J, Bache RJ, Merkus D & Duncker DJ (2012). Peripheral circulation. Compr Physiol 2, 321–447. [PubMed: 23728977]

Li Y, Wei Y, Zhang F, Wang D & Wu X (2012). Changes in the pharmacokinetics of glibenclamide in rats with streptozotocin-induced diabetes mellitus. Acta Pharmaceutica Sinica B 2, 198–204.

Lu S, Xiang L, Clemmer JS, Gowdey AR, Mittwede PN & Hester RL (2013). Impaired vascular K_{ATP} function attenuates exercise capacity in obese Zucker rats. Microcirculation 20, 662–669. [PubMed: 23647569]

Marcondes FJ, Bianchi FJ & Tanno AP (2002). Determination of the estrous cycle phases of rats: some helpful considerations. Brazilian J Biol 62, 609–614.

Matar W, Nosek TM, Wong D & Renaud JM (2000). Pinacidil suppresses contractility and preserves energy but glibenclamide has no effect during muscle fatigue. Am J Physiol Cell Physiol 278, C404–C416. [PubMed: 10666037]

McAlister FA, Eurich DT, Majumdar SR & Johnson JA (2008). The risk of heart failure in patients with type 2 diabetes treated with oral agent monotherapy. Eur J Heart Fail 10, 703–708. [PubMed: 18571471]

McDonough P, Behnke BJ, Kindig CA & Poole DC (2001). Rat muscle microvascular PO_2 kinetics during the exercise off-transient. Exp Physiol 86, 349–356. [PubMed: 11429652]

McDonough P, Behnke BJ, Padilla DJ, Musch TI & Poole DC (2005). Control of microvascular oxygen pressures in rat muscles comprised of different fibre types. J Physiol 563, 903–913. [PubMed: 15637098]

Monod H & Scherrer J (1965). The work capacity of a synergic muscular group. Ergonomics 8, 329–338.

Montvida O, Shaw J, Atherton JJ, Stringer F & Paul SK (2018). Long-term trends in antidiabetes drug usage in the U.S.: real-world evidence in patients newly diagnosed with type 2 diabetes. Diabetes Care 41, 69–78. [PubMed: 29109299]

Musch TI (1988). Measurements of metabolic rate in rats: a comparison of techniques. J Appl Physiol 65, 964–970. [PubMed: 3139623]

Musch TI (1992). Training effects on the regional blood flow response to exercise in myocardial infarcted rats. Am J Physiol-Heart C 262, H1846–H1852.

Musch TI & Terrell JA (1992). Skeletal muscle blood flow abnormalities in rats with a chronic myocardial infarction: rest and exercise. Am J Physiol Heart Circ Physiol 262, H411–H419.

Musch TI, Moore RL, Leathers DJ, Bruno A & Zelis R (1986). Endurance training in rats with chronic heart failure induced by myocardial infarction. Circulation 74, 431–441. [PubMed: 3731431]

Padilla DJ, McDonough P, Behnke BJ, Kano Y, Hageman KS, Musch TI & Poole DC (2006). Effects of type II diabetes on capillary hemodynamics in skeletal muscle. Am J Physiol Heart Circ Physiol 291, H2439–H2444. [PubMed: 16844923]

Padilla DJ, McDonough P, Behnke BJ, Kano Y, Hageman KS, Musch TI & Poole DC (2007). Effects of type II diabetes on muscle microvascular oxygen pressures. Respir Physiol Neurobiol 156, 187–195. [PubMed: 17015044]

Poole DC (2019). Edward F. Adolph distinguished lecture. Contemporary model of muscle microcirculation: gateway to function and dysfunction. J Appl Physiol 127, 1012–1033. [PubMed: 31095460]

Poole DC, Burnley M, Vanhatalo A, Rossiter HB & Jones AM (2016). Critical power: an important fatigue threshold in exercise physiology. Med Sci Sports Exerc 48, 2320–2334. [PubMed: 27031742]

Poole DC, Copp SW, Colburn TD, Craig JC, Allen DL, Sturek M, O'Leary DS, Zucker IH & Musch TI (2020). Guidelines for animal exercise and training protocols for cardiovascular studies. Am J Physiol Heart Circ Physiol 318, H1100–H1138. [PubMed: 32196357]

Poole DC, Copp SW, Ferguson SK & Musch TI (2013). Skeletal muscle capillary function: contemporary observations and novel hypotheses. Exp Physiol 98, 1645–1658. [PubMed: 23995101]

Poole DC & Jones AM (2012). Oxygen uptake kinetics. Compr Physiol 2, 933–996. [PubMed: 23798293]

Poole DC, Ward SA, Gardner GW & Whipp BJ (1988). Metabolic and respiratory profile of the upper limit for prolonged exercise in man. Ergonomics 31, 1265–1279. [PubMed: 3191904]

Richardson RS, Noyszewski EA, Leigh JS & Wagner PD (1998). Lactate efflux from exercising human skeletal muscle: role of intracellular PO_2. J Appl Physiol 85, 627–634. [PubMed: 9688741]

Richardson RS, Poole DC, Knight DR, Kurdak SS, Hogan MC, Grassi B, Johnson EC, Kendrick KF, Erickson BK & Wagner PD (1993). High muscle blood flow in man: is maximal O_2 extraction compromised? J Appl Physiol 75, 1911–1916. [PubMed: 8282650]

Richmond KN, Shonat RD, Lynch RM & Johnson PC (1999). Critical PO_2 of skeletal muscle in vivo. Am J Physiol Heart Circ Physiol 277, H1831–H1840.

Roca J, Agusti AG, Alonsa A, Poole DC, Viegas C, Barbera JA, Rodriguez-Roisin R, Ferrer A & Wagner PD (1992). Effect of training on muscle O_2 transport at VO_2max. J Appl Physiol 73, 1067–1076. [PubMed: 1400019]

Rosenberry R, Tucker WJ, Haykowsky MJ, Trojacek D, Chamseddine HH, Arena-Marshall CA, Zhu Y, Wang J, Kellawan JM, Tian F & Nelson MD (2019). Determinants of skeletal muscle oxygen consumption assessed by near-infrared diffuse correlation spectroscopy during incremental handgrip exercise. J Appl Physiol 127, 698–706. [PubMed: 31318612]

Rumsey WL, Vanderkooi JM & Wilson DF (1988). Imaging of phosphorescence: a novel method for measuring oxygen distribution in perfused tissue. Science 241, 1649–1651, 1988. [PubMed: 3420417]

Saito Y, McKay M, Eraslan A & Hester RL (1996). Functional hyperemia in striated muscle is reduced following blockade of ATP-sensitive potassium channels. Am J Physiol Heart Circ Physiol 270, H1649–H1654.

Simpson SH, Lee J, Choi S, Vandermeer B, Abdelmoneim AS & Featherstone TR (2015). Mortality risk among sulfonylureas: a systematic review and network meta-analysis. Lancet Diabetes Endocrinol 3, 43–51. [PubMed: 25466239]

Simpson SH, Majumdar SR, Tsuyuki RT, Eurich DT & Johnson JA (2006). Dose-response relation between sulphonylurea drugs and mortality in type 2 diabetes mellitus: a population-based cohort study. CMAJ 174, 169–174. [PubMed: 16415461]

Smith JR, Hageman KS, Harms CA, Poole DC & Musch TI (2017). Respiratory muscle blood flow during exercise: Effects of sex and ovarian cycle. J Appl Physiol 122, 918–924. [PubMed: 28126910]

Thabet M, Miki T, Seino S & Renaud TM (2005). Treadmill running causes significant fiber damage in skeletal muscle of K_{ATP} channel-deficient mice. Physiol Genomics 22, 204–212. [PubMed: 15914579]

Van Oosterhout MFM, Prinzen FW, Sakurada S, Glenny RW & Hales JRS (1998). Fluorescent microspheres are superior to radioactive microspheres in chronic blood flow measurements. Am J Physiol-Heart C 275, H110–H115.

Wagner PD (1992). Gas exchange and peripheral diffusion limitation. Med Sci Sports Exerc 24, 54–58. [PubMed: 1548996]

Wagner PD (1996). Determinants of maximal oxygen transport and utilization. Annu Rev Physiol 58, 21–50. [PubMed: 8815793]

Wilson DF, Erecinska M, Drown C & Silver IA (1977). Effect of oxygen tension on cellular energetics. Am J Physiol Cell Physiol 233, C135–C140.

Zingman LV, Alekseev AE, Hodgson-Zingman DM & Terzic A (2007). ATP-sensitive potassium channels: metabolic sensing and cardioprotection. J Appl Physiol 103, 1888–1893. [PubMed: 17641217]

Key points

- Oral sulphonylureas, widely prescribed for diabetes, inhibit pancreatic ATP-sensitive K^+ (K_{ATP}) channels to increase insulin release. However, K_{ATP} channels are also located within vascular (endothelium and smooth muscle) and muscle (cardiac and skeletal) tissue.
- We evaluated left ventricular function at rest, maximal aerobic capacity $\left(\dot{V}O_2max\right)$ and submaximal exercise tolerance (i.e. speed–duration relationship) during treadmill running in rats, before and after systemic K_{ATP} channel inhibition via glibenclamide.
- Glibenclamide impaired critical speed proportionally more than $\dot{V}O_2max$ but did not alter resting cardiac output.
- Vascular K_{ATP} channel function (topical glibenclamide superfused onto hindlimb skeletal muscle) resolved a decreased blood flow and interstitial PO_2 during twitch contractions reflecting impaired O_2 delivery-to-utilization matching.
- Our findings demonstrate that systemic K_{ATP} channel inhibition reduces $\dot{V}O_2max$ and critical speed during treadmill running in rats due, in part, to impaired convective and diffusive O_2 delivery, and thus $\dot{V}O_2$, especially within fast-twitch oxidative skeletal muscle.

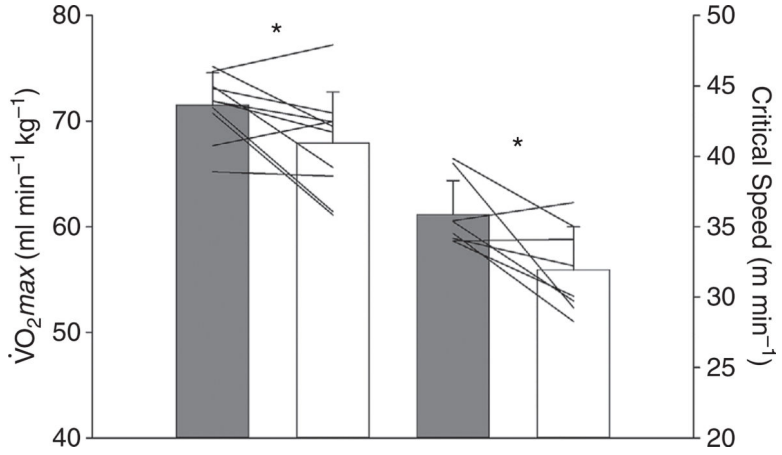

Figure 1. Effect of systemic K_{ATP} channel inhibition on maximal and submaximal exercise

Note the significant reduction in maximal oxygen uptake ($\dot{V}O_2max$; $n = 10$) and critical speed ($n = 8$) following glibenclamide (open bars) compared with control (grey bars). Data are means ± SD with individual data plotted and compared via two-tail paired *t* tests. *$P < 0.05$ *vs.* control.

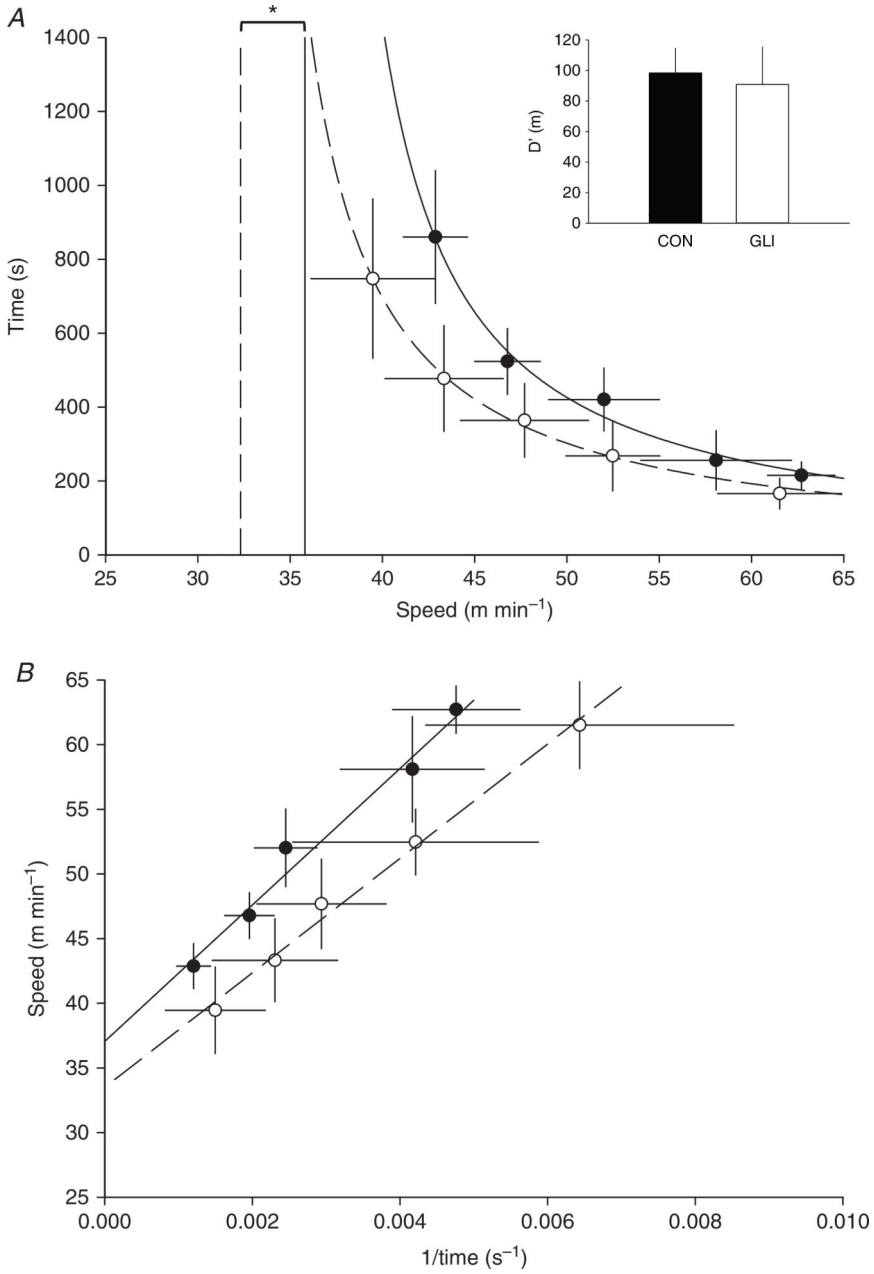

Figure 2. Speed–duration relationship following systemic K_{ATP} channel inhibition

The hyperbolic (*A*) and 1/time linear (*B*) speed–duration relationships are modelled under control (closed circle, continuous line) and systemic K_{ATP} channel inhibition (GLI; open circle, dashed line) conditions to determine critical speed (vertical lines (*A*) and *y*-intercept (*B*)) and D′ (inset). These mean data fits are for illustrative purposes only, with individually determined critical speed and D′ and subsequent group means presented in Table 2. Data are means ± SD and compared via two-tail paired *t* tests.

* $P < 0.05$ *vs.* control.

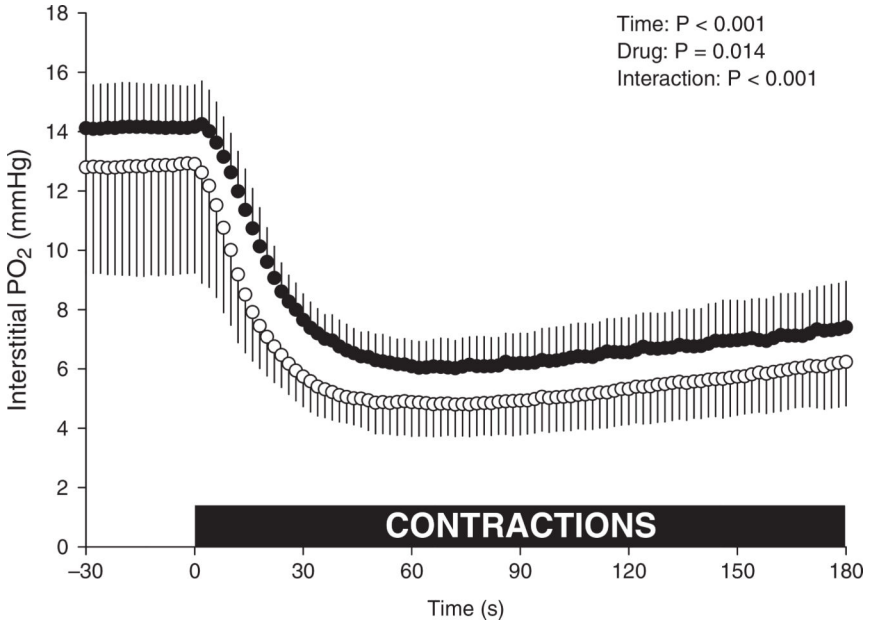

Figure 3. Interstitial PO_2 of fast-twitch oxidative muscle following local K_{ATP} channel inhibition

Note the difference in mixed gastrocnemius PO_2*is* following glibenclamide (GLI, open symbols, $n = 10$) superfusion compared with control (closed symbols). Dashed line denotes the onset of twitch contractions at time zero. Data are means ± SD and compared via two-way (Time × Drug) repeated measure ANOVA with Tukey's *post hoc* analyses.

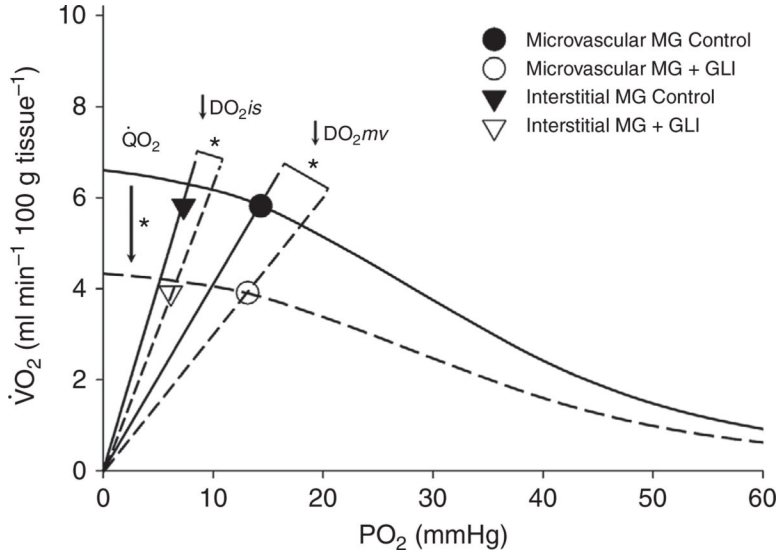

Figure 4. The effect of local K_{ATP} channel inhibition on the convective and diffusive determinants of oxygen transport

Graphical representation of the relationship between convective ($\dot{V}O_2 = \dot{Q} \times$ a-vO_2 difference; curved line) and diffusive ($\dot{V}O_2 = DO_2 \times PO_2$; slope from origin) determinants of oxygen transport in the microvascular (circles) and interstitial (down triangles) compartments of the fast-twitch oxidative mixed gastrocnemius (MG, $n = 10$) muscle following vascular K_{ATP} channel inhibition via glibenclamide (GLI, open symbols). Importantly, unlike haemoglobin–O_2 transport in the microvasculature, the lack of haeme–O_2 storage in interstitial fluid dictates that interstitial $\dot{V}O_2$ ($\dot{V}O_2is$) must equal microvascular $\dot{V}O_2$ ($\dot{V}O_2mv$) allowing DO_2is to be assessed with the present data $\left(\dot{V}O_2mv = \dot{V}O_2i\ s = DO_2is \times PO_2is\right)$. Note the reductions in both convective (QO_2mv, curved lines *y*-intercept) and diffusive (DO_2mv and DO_2is) components of MG muscle compared with control (closed symbols). $*P < 0.05$ *vs.* control with two-tail paired *t* tests

Table 1.

Doppler echocardiographic assessment of left ventricular function during control and systemic K_{ATP} channel inhibition

	Control	Glibenclamide
LVIDd (cm)	0.71 ± 0.08	0.72 ± 0.05
LVIDs (cm)	0.38 ± 0.08	0.41 ± 0.06
FS (%)	47 ± 6	42 ± 5
LVEDV (ml)	0.83 ± 0.24	0.83 ± 0.18
LVESV (ml)	0.15 ± 0.07	0.19 ± 0.09
SV (ml)	0.68 ± 0.19	0.65 ± 0.11
EF (%)	83 ± 5	78 ± 6
+V (cm s^{-1})	2.76 ± 0.49	2.44 ± 0.43
−V (cm s^{-1})	2.11 ± 0.59	1.70 ± 0.23 *
HR (bpm)	321 ± 23	304 ± 22 *
CO (ml min^{-1})	219 ± 64	197 ± 39

LVIDd, left ventricular end-diastole internal diameter; LVIDs, left ventricular end-systole internal diameter; FS, fractional shortening; LVEDV, left ventricular end-diastolic volume; LVESV, left ventricular end-systolic volume; SV, stroke volume; EF, ejection fraction; +V, rate of contraction; −V, rate of relaxation; HR, heart rate; CO, cardiac output. Data are means ± SD ($n = 10$) and compared via two-tail paired t test.

* $P < 0.05$ *vs.* control.

Table 2.

Individual maximal oxygen uptake and speed–duration relationship parameters during control and systemic K_{ATP} channel inhibition

	Control			Glibenclamide		
	$\dot{V}O_2max$	CS (m min^{-1})	D′ (m)	$\dot{V}O_2max$	CS (m min^{-1})	D′ (m)
1	67.7	39.5	84	70.0	29.3	124
2	71.3	34.2	127	61.4	32.2	79
3	75.2	34.5	93	69.5	28.3	95
4	65.2	–	–	64.8	–	–
5	70.8	34.0	92	61.1	34.1	83
6	73.3	39.8	75	65.5	35.0	79
7	74.7	35.4	101	77.2	29.7	127
8	73.1	–	–	70.8	–	–
9	71.9	34.0	111	69.9	30.1	89
10	71.9	35.4	105	69.0	36.7	52
Mean ± SD	71.5 ± 3.1	35.9 ± 2.4	98 ± 16	67.9 ± 4.8 *	31.9 ± 3.1 *	91 ± 25

$\dot{V}O_2max$, maximal oxygen uptake; CS, critical speed; D′, curvature constant. The speed–duration relationship parameters are presented from the hyperbolic model. Data were compared via two-tail paired *t* tests.

* $P < 0.05$ *vs.* control.

Table 3.

Interstitial PO_2 kinetics parameters during 180 s twitch contractions and 240 s recovery during control and local K_{ATP} channel inhibition

	Mixed gastrocnemius	
	Control	**Glibenclamide**
Pre-superfusion PO_2is (mmHg)	–	13.8 ± 3.4
PO_2is_{BL} (mmHg)	14.1 ± 1.4	12.8 ± 3.6 *
Δ_1PO_2is (mmHg)	8.2 ± 1.5	8.1 ± 3.1
TD (s)	8.0 ± 4.3	5.2 ± 3.2 *
τ (s)	14.1 ± 2.7	12.2 ± 3.0
MRT (s)	22.2 ± 4.7	17.3 ± 4.3 *
PO_2is_{nadir} (mmHg)	5.9 ± 0.9	4.7 ± 1.1 *
Δ_2PO_2is (mmHg)	1.4 ± 0.9	1.4 ± 0.8
PO_2is_{end} (mmHg)	7.3 ± 1.5	6.1 ± 1.4
Δ_1PO_2is/τ (mmHg s^{-1})	0.60 ± 0.16	0.72 ± 0.36
Recovery T_{63} (s)	95 ± 19	118 ± 20 *
Recovery PO_2is (mmHg)	14.6 ± 4.0	15.3 ± 6.5
Δ_3PO_2is/T_{63} (mmHg s^{-1})	0.07 ± 0.03	0.08 ± 0.04

PO_2is_{BL}, resting baseline; PO_2is; Δ_1PO_2is and Δ_2PO_2is, amplitude of the first and second components, respectively; TD, time delay; τ, time constant; MRT, mean response time; PO_2is_{nadir}, lowest response prior to secondary rise in PO_2is; PO_2is_{end}, PO_2is at the end of contractions; Δ_1PO_2is/τ, rate of PO_2is fall; T_{63}, time to reach 63% of final response; Δ_3PO_2is/T_{63}, rate of PO_2is recovery. Data are means ± SD and compared via two-tail paired *t* tests.

* $P < 0.05$ *vs.* control.